


Low-Carrier-Density Sputtered MoS₂ Film by Vapor-Phase Sulfurization

KENTARO MATSUURA ^{1,3}, TAKUMI OHASHI,¹ IRIYA MUNETA,¹
SEIYA ISHIHARA,² KUNYUKI KAKUSHIMA,¹ KAZUO TSUTSUI,¹
ATSUSHI OGURA,² and HITOSHI WAKABAYASHI¹

1.—Tokyo Institute of Technology, Yokohama 226-8502, Kanagawa, Japan. 2.—Meiji University, Kawasaki 214-5871, Kanagawa, Japan. 3.—e-mail: matsuura.k.ae@m.titech.ac.jp

Sulfurization with sulfur vapor has been demonstrated to be useful for fabricating sputtered-multilayer MoS₂ films with an approximately 4-nm thickness. With this process, sulfur vacancies in the sputtered MoS₂ films were remarkably compensated, and MoO₃ was simultaneously sulfurized. Eventually, carrier densities of the sulfurized MoS₂ films were successfully reduced to $1.8 \times 10^{16} \text{ cm}^{-3}$ and electron mobilities were considerably enhanced to $25.2 \text{ cm}^2/\text{V}\cdot\text{s}$.

Key words: Transition metal di-chalcogenide, molybdenum disulfide, sputtering, vapor-phase sulfurization, carrier density

INTRODUCTION

Transition metal di-chalcogenides (TMDCs) have attracted remarkable attention because of their excellent electrical and optical properties, which are suitable for fabricating not only three-dimensional integrated circuits but also flexible and optoelectronic devices. Molybdenum disulfide (MoS₂) is the most promising candidate among TMDCs because of its transparency, flexibility, and high mobility ($\sim 700 \text{ cm}^2/\text{V}\cdot\text{s}$) even with thin atom layers.^{1–3} For example, MoS₂ has appropriate energy band gaps of 1.9 eV and 1.2 eV in its monolayers and multilayers, respectively.^{4,5} However, it is difficult to synthesize large and uniform MoS₂ films using reported methods such as exfoliation and chemical vapor deposition (CVD). Although it is possible to achieve good-quality MoS₂ thin films using the exfoliation method,^{1–3,6} the resulting films have higher carrier densities of up to 10^{20} cm^{-3} ⁷ owing to contamination with alkali metals.⁸ In addition, with CVD, the MoS₂ film forms triangular structures at random positions because of the uncontrollable sites of nucleation and its lattice structure.^{9–15} To enlarge the

grain size of MoS₂ films, it is necessary to coat a polymer such as perylene-3,4,9,10-tetracarboxylic acid tetra-potassium salt (PTAS) onto the SiO₂ substrate directly.¹² This potassium-containing polymer leads to the Fermi-level pinning near the conduction band minimum.⁸

Therefore, we selected a sputtering process using an MoS₂ target to synthesize uniform and large-area MoS₂ films to avoid alkali contamination.^{16–23} However, sulfur vacancies were formed even in the sputtered film.²⁴ In monolayer MoS₂ film, these sulfur vacancies are classified as dopants because the sulfur vacancies generate energy states at 0.2 eV, near the conduction band minimum.^{23,25} This consequently leads to higher carrier density and depletion mode operation in accumulation transistors. Therefore, compensation for the sulfur vacancies is required, as demonstrated in Refs. 18, 19, and 24. By using MoS₂ compound target in Ar atmosphere during sputtering, it is possible to deposit MoS₂ thin film with less chamber contamination. Although no metals were deposited by sputtering in this study, metals are going to be sputtered after MoS₂ sputtering and sulfurization. Accordingly, reducing contamination is important to deposited pure metal at an industrial scale.²⁶ Therefore, we adopted a separate process of sputtering and sulfurization.

In this study, we aimed to aggressively compensate for sulfur vacancies and decrease the carrier density by sulfurization, for obtaining both *n*- and *p*-field-effect transistors (FETs) with normally off operation in the accumulation mode.

EXPERIMENTS

Figures 1 and 2 show the process flow and cross-sectional structure of the MoS₂ sample, respectively. An MoS₂ film was deposited on an SiO₂/Si substrate using an ultra-high vacuum (UHV) radio frequency (RF) magnetron sputtering system under the following conditions: 80 mm ϕ MoS₂ target (99.79% pure); RF power of 50 W; a distance between the MoS₂ target and the substrate of 150 mm; argon partial pressure of 0.55 Pa; substrate temperature of 300°C. Figure 3a and b shows schematic diagrams of the sulfurization process and temperature sequence, respectively. The sputtered MoS₂ film was annealed at 300°C, 400°C, 500°C, 600°C, and 700°C in sulfur vapor made from sulfur powder evaporated at 200°C, carried by Ar gas flowing at a rate of 1000 sccm at 100 kPa, 300 kPa, and 10 kPa. After the sulfurization, the thickness of MoS₂ film was approximately 4 nm, confirmed by transmission electron microscopy (TEM). In the sulfurization process, two heaters were used, designated 1 and 2, as shown in Fig. 3a. The sulfur powder and sputtered MoS₂ film were placed in a quartz tube. The sulfur powder and the samples were evaporated by heater 2 and annealed by heater 1. The temperature of heater 2 was set to 200°C and the temperature of heater 1 was varied. As shown in Fig. 3b, this process is divided into three time domains, which consist of (a) ramping up the temperatures of heaters 1 and 2 to 700°C and 200°C, respectively, under an Ar flow rate of 1000 sccm, (b) sulfurization for 10 min, and (c) ramping down the temperature with an increase in the Ar gas flow rate to 1500 sccm over 10 min in order to evacuate the sulfur vapor quickly.

For physical evaluation of the MoS₂ films, Raman spectroscopy was performed at a wavelength of

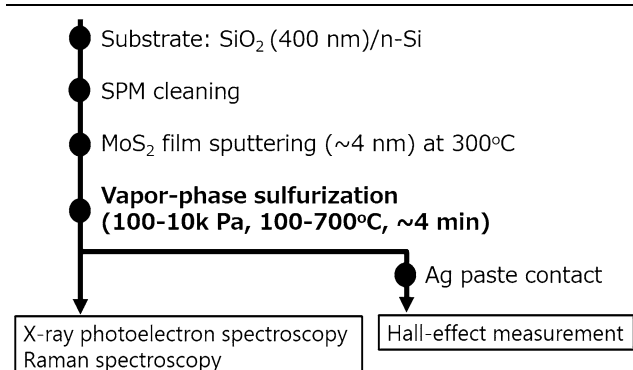


Fig. 1. Process flow and measurement methods.

532 nm. X-ray photoelectron spectroscopy (XPS) was also performed using an Al K _{α} x-ray source. The Voigt function (x) was used to fit the x-ray photoelectron spectra of the MoS₂ films. A composition ratio of the MoS₂ film was expressed as shown in the following equation:

$$C_i = \frac{A_i/\text{RSF}_i}{\sum_j A_j/\text{RSF}_j} \times 100 \quad (1)$$

where C_i is the composition ratio, A_i is the peak area, and RSF_i is the relative sensitivity factor of the atom i . Hall-effect measurements were performed on the sputtered MoS₂ film. Silver paste was

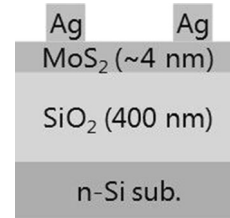


Fig. 2. Cross-sectional structure of the MoS₂ sample.

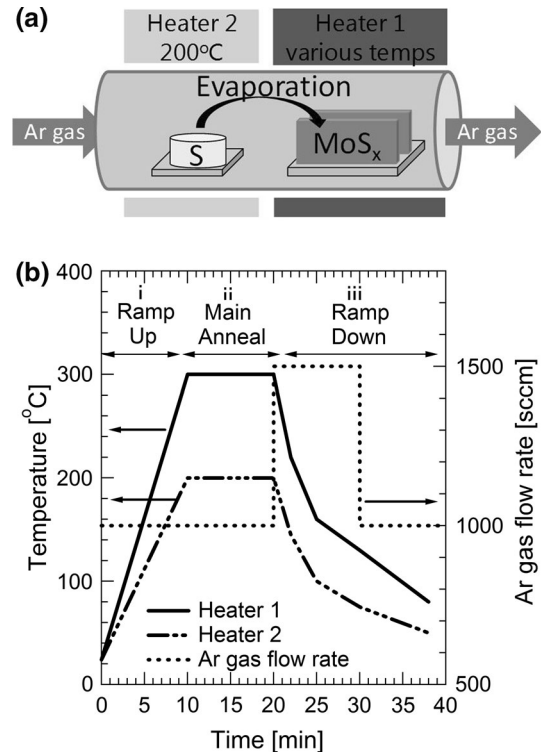


Fig. 3. Sulfurization process using (a) a quartz tube with two heaters, (b) time sequence of the temperature and gas flow rate, when heaters 1 and 2 were set to 300°C and 200°C, respectively.

attached to four corners as a metal contact, as shown in Fig. 2.

RESULTS AND DISCUSSION

Figure 4 shows the Raman peak intensity dependence on pressure. The large dashed line at this center of the figure indicates the boiling point of the sulfur powder at 200°C. In this figure, the Raman peak intensities were successfully enhanced when

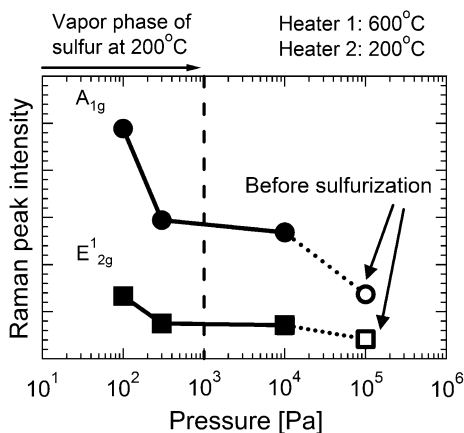


Fig. 4. Raman peak intensity of A_{1g} and E_{2g}^1 as a function of pressure for the approximately 4-nm-thick MoS₂ film.

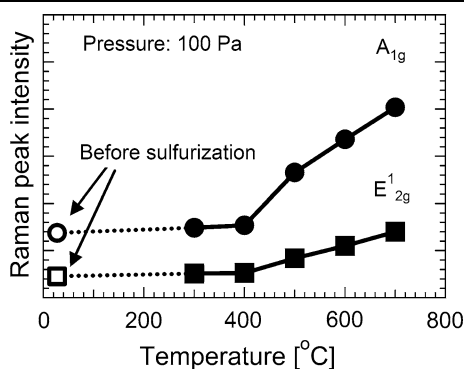


Fig. 5. Raman peak intensity of A_{1g} and E_{2g}^1 as a function of temperature for the approximately 4-nm-thick MoS₂ film at 100 Pa.

the pressure decreased below 1000 Pa. This is because the sulfur powder in the quartz tube transitioned into the vapor phase with a decrease in pressure below 1000 Pa even at 200°C.^{27,28}

Accordingly, we evaluated the temperature dependence of sulfurization by Raman spectroscopy and XPS at 100 Pa. Figure 5 shows the Raman peak intensity, and Fig. 6a and b indicates the full-width at half maximum (FWHM) value of both A_{1g} (out-of-plane mode vibration of sulfur) and E_{2g}^1 (in-plane vibration mode of sulfur and molybdenum) from the Raman spectra when the temperature was raised to 700°C. As can be seen in these figures, as the temperature rises, the Raman peak intensities increase and the FWHM decreases. These indicate that the sulfurization of the sulfur vapor is enhanced at higher temperatures and sulfur annealing was shown to improve the crystallinity of the sputtered MoS₂ film. As a result, the FWHM decreases to 7–8 cm⁻¹. The FWHM of the MoS₂ film on SiO₂ fabricated by CVD is approximately 6 cm⁻¹.¹¹ Therefore, the crystallinity of the sputtered MoS₂ film is comparable to that of the CVD MoS₂ film. Figure 7a and b shows the x-ray photoelectron spectra of molybdenum 3d and sulfur 2s for the as-sputtered films sulfurized at 700°C, respectively. As shown in Fig. 7a, peaks arising from Mo–S bonds are observed, which are speculated to be in the form of an MoS₂ crystal. However, peaks arising from Mo–O bonds are also observed, and this can be due to the presence of MoO₃.^{21,22} This means that the as-sputtered MoS₂ film is oxidized after the sputtering process, in agreement with previous reports.^{29,30} Comparing Fig. 7a and b, both the peaks corresponding to Mo–Mo and Mo–O decrease in intensity and those corresponding to Mo–S increase in intensity simultaneously during the sulfurization process. It is speculated that the Mo–Mo bonding related to sulfur vacancies is sulfurized and transformed toward MoS₂ film, and MoO₃ is simultaneously reduced toward MoS₂ film. Moreover, Fig. 8a and b shows the x-ray photoelectron spectra of the sulfur 2p orbital for the as-sputtered films sulfurized at 700°C, respectively. Prior to sulfurization, peaks due to S–Mo chemical bonding

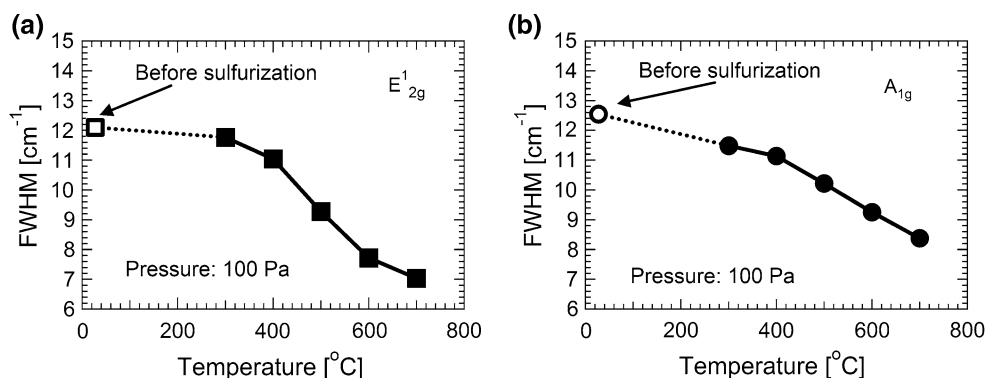


Fig. 6. FWHM of (a) A_{1g} and (b) E_{2g}^1 as a function of temperature for the approximately 4-nm-thick MoS₂ film at 100 Pa.

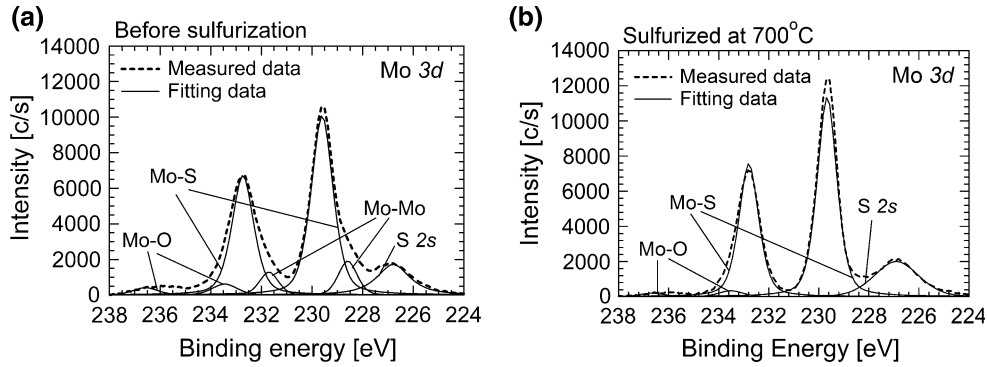


Fig. 7. XPS spectra of molybdenum 3d of (a) the as-sputtered film and (b) the sulfurized film at 700°C.

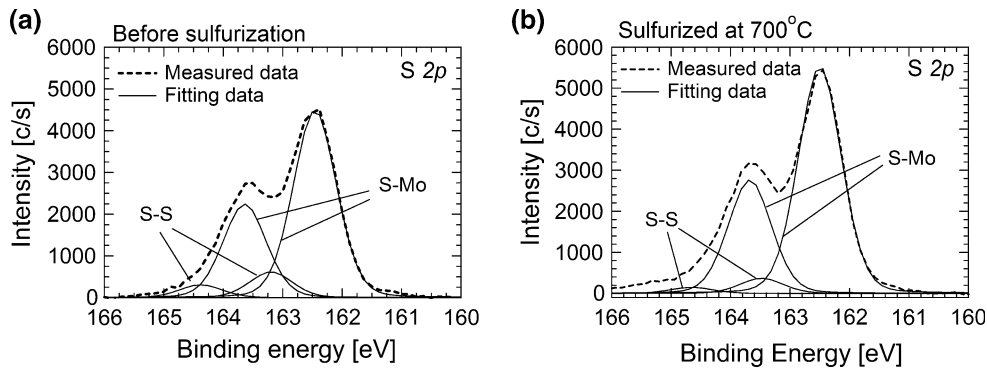


Fig. 8. X-ray photoelectron spectra of sulfur 2p for (a) the as-sputtered film and (b) the sulfurized film at 700°C.

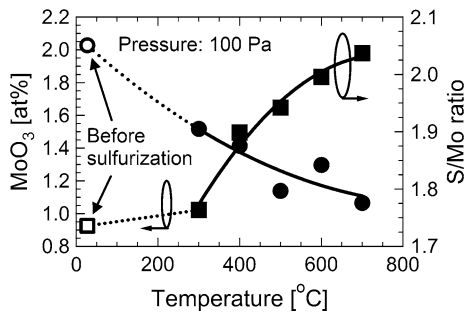


Fig. 9. MoO_3 contents determined from the Mo–O peak area and S-to-Mo ratio of the MoS_2 film determined from the Mo–S and S–Mo peak areas in x-ray photoelectron spectra for the approximately 4-nm-thick MoS_2 film shown in Figs. 7 and 8.

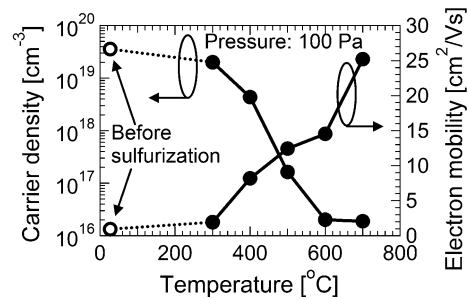


Fig. 10. Hall-effect measurement results of carrier density and electron mobility for approximately 4-nm-thick MoS_2 film as function of temperature at 100 Pa.

are observed, which possibly arise from the MoS_2 film. Compared to Fig. 8b, the S–Mo peaks increase due to the introduction of sulfur vapor, causing a simultaneous reduction in the non-bonding Mo and MoO_3 contributions. In contrast, S–S peaks appearing just after sputtering^{18,19} decrease because sulfur residues in the sputtered film are successfully reduced by the sulfurization process sequence. These results are consistent with those shown in Fig. 7. As seen in Fig. 8b, even after sulfurization, a small amount of non-bonding sulfur remains. Therefore, higher vacuum ambient and longer evacuation time are required until the temperature is

sufficiently reduced. Furthermore, as shown in Fig. 9, the MoO_3 content in the MoS_2 film, as calculated from peak area, is reduced by the sulfurization process.

Moreover, the S-to-Mo composition ratios of the MoS_2 film calculated from Mo–S and S–Mo peak areas in the x-ray photoelectron spectra increase with an increase in temperature, reaching a ratio of approximately 2.0 in Fig. 9. Eventually, this sulfurization results in not only the reduction of MoO_3 , but the sulfurization toward MoS_2 film. Figure 10 shows the results of the Hall-effect measurements of carrier density and electron mobility. The carrier

density decreases to $1.8 \times 10^{16} \text{ cm}^{-3}$ monotonically. It is speculated that the number of sulfur vacancies, which act as donors, is remarkably reduced by sulfurization. The electron mobility simultaneously increases up to a maximum of $25.2 \text{ cm}^2/\text{V}\cdot\text{s}$. It was confirmed that the electrical properties of the sputtered MoS₂ film were successfully improved by the sulfurization process. In previous study, it was reported the carrier density of thin film MoS₂ made by the exfoliation method and CVD is approximately 10^{20} cm^{-3} and 10^{18} cm^{-3} , respectively.^{7,31} It is found that the carrier density of sputtered MoS₂ thin film becomes lower than reported methods by this sulfurization process. Thus, reduction of sulfur vacancies within the MoS₂ film is essential for achieving an intrinsic semiconductor MoS₂ film.

CONCLUSION

We aimed to compensate for sulfur vacancies in a sputtered MoS₂ film by vapor-phase sulfurization. Sulfur vacancy compensation and improvements in crystallinity were achieved with a decrease in pressure to 100 Pa and an increase in temperature to 700°C. The composition ratio of the sputtered MoS₂ increased and the carrier density decreased to $1.8 \times 10^{16} \text{ cm}^{-3}$ with sulfurization. This indicated that the sulfur vacancies acting as dopants decreased. This carrier density is lower than that of reported processes, exfoliation, or CVD. It is concluded that this sulfurization process is promising for the realization of intrinsic channels of *n*- and *p*-FETs for normally off operation in the accumulation mode.

ACKNOWLEDGEMENTS

This work was partly supported by JST CREST, grant nos. JPMJCR16F4, JST COI and JSPS KAKENHI grant no. 26105014.

REFERENCES

- S. Das, H.-Y. Chen, A.V. Penumatcha, and J. Appenzeller, *Nano Lett.* 13, 100 (2013).
- B. Radisavljevic, A. Radenovic, J. Brivio, V. Giacometti, and A. Kis, *Nat. Nanotechnol.* 6, 147 (2011).
- H. Wang, L. Yu, Y.-H. Lee, Y. Shi, A. Hsu, M.L. Chin, L.-J. Li, M. Dubey, J. Kong, and T. Palacios, *Nano Lett.* 12, 4674 (2012).
- K.F. Mak, C. Lee, J. Hone, J. Shan, and T.F. Heinz, *Phys. Rev. Lett.* 105, 136805 (2010).
- A. Splendiani, L. Sun, Y. Zhang, T. Li, J. Kim, C.-Y. Chim, G. Galli, and F. Wang, *Nano Lett.* 10, 1271 (2010).
- J.N. Coleman, M. Lotya, A. O'Neill, S.D. Bergin, P.J. King, U. Khan, K. Young, A. Gaucher, S. De, R.J. Smith, I.V. Shvets, S.K. Arora, G. Stanton, H.Y. Kim, K. Lee, G.T. Kim, G.S. Duesberg, T. Hallam, J.J. Boland, J.J. Wang, J.F. Donegan, J.C. Grunlan, G. Moriarty, A. Shmeliov, R.J. Nicholls, J.M. Perkins, E.M. Grievson, K. Theuwissen, D.W. McComb, P.D. Nellist, and V. Nicolosi, *Science* 331, 568 (2011).
- B. Radisavljevic and A. Kis, *Nat. Mater.* 12, 815 (2013).
- K. Dolui, I. Rungger, C.D. Pemmaraju, and S. Sanvito, *Phys. Rev. B* 88, 075420 (2013).
- A.M. van der Zande, P.Y. Huang, D.A. Chenet, T.C. Berkelbach, Y. You, G.H. Lee, T.F. Heinz, D.R. Reichman, D.A. Muller, and J.C. Hone, *Nat. Mater.* 12, 554–561 (2013).
- D. Dumcenco, D. Ovchinnikov, O.L. Sanchez, P. Gillet, D.T.L. Alexander, S. Lazar, A. Radenovic, and A. Kis, *2D Mater* 2, 4 (2015).
- W. Wu, D. De, S.-C. Chang, Y. Wang, H. Peng, J. Bao, and S.-S. Pei, *Appl. Phys. Lett.* 102, 142106 (2013).
- J. Park, N. Choudhary, J. Smith, G. Lee, M. Kim, and W. Choi, *Appl. Phys. Lett.* 106, 012104 (2015).
- Y.H. Lee, X.Q. Zhang, W. Zhang, M.T. Chang, C.T. Lin, K.D. Chang, Y.C. Yu, J.T.W. Wang, C.S. Chang, L.J. Li, and T.W. Lin, *Adv. Mater.* 24, 2320 (2012).
- S. Wang, M. Pacios, H. Bhaskaran, and J.H. Warner, *Nanotechnology* 27, 085604 (2016).
- S.-S. Pei, L. Yu, H. Wang, W. Fang, X. Ling, Y. Shi, C.T. Lin, J.K. Huang, M.T. Chang, C.S. Chang, M. Dresselhaus, T. Palacios, L.J. Li, and J. Kong, *Nano Lett.* 13, 1852–1857 (2013).
- T. Ohashi, K. Suda, S. Ishihara, N. Sawamoto, S. Yamaguchi, K. Matsuura, K. Kakushima, N. Sugii, A. Nishiyama, Y. Kataoka, K. Natori, K. Tsutsui, H. Iwai, A. Ogura, and H. Wakabayashi, *Jpn. J. Appl. Phys.* 54, 04DN08 (2015).
- T. Ohashi, I. Muneta, K. Matsuura, S. Ishihara, Y. Hibino, N. Sawamoto, K. Kakushima, K. Tsutsui, A. Ogura, and H. Wakabayashi, *Appl. Phys. Exp.* 10, 4 (2017).
- J. Shimizu, T. Ohashi, K. Matsuura, I. Muneta, K. Kakushima, K. Tsutsui, and H. Wakabayashi, *Jpn. J. Appl. Phys.* 56, 04CP06 (2017).
- J. Shimizu, T. Ohashi, K. Matsuura, I. Muneta, K. Kakushima, K. Tsutsui, N. Ikarashi, and H. Wakabayashi, *Electron Dev. Technol. Manuf. (EDTM)* P-22, 0110 (2017).
- S. Ishihara, Y. Hibino, N. Sawamoto, T. Ohashi, K. Matsuura, H. Machida, M. Ishikawa, H. Wakabayashi, and A. Ogura, *ECS J. Solid State Sci. Technol.* 5, Q3012 (2016).
- S. Ishihara, K. Suda, Y. Hibino, N. Sawamoto, T. Ohashi, S. Yamaguchi, K. Matsuura, H. Machida, M. Ishikawa, H. Sudoh, H. Wakabayashi, and A. Ogura, *MRS Proc.* 1781, 11 (2015).
- S. Ishihara, Y. Hibino, N. Sawamoto, K. Suda, T. Ohashi, K. Matsuura, H. Machida, M. Ishikawa, H. Sudoh, H. Wakabayashi, and A. Ogura, *Jpn. J. Appl. Phys.* 55, 04EJ07 (2016).
- S. Ishihara, Y. Hibino, N. Sawamoto, K. Suda, T. Ohashi, K. Matsuura, H. Machida, M. Ishikawa, H. Sudoh, H. Wakabayashi, and A. Ogura, *Jpn. J. Appl. Phys.* 55, 06GF01 (2016).
- S. Tongay, J. Suh, C. Ataca, W. Fan, A. Luce, J.S. Kang, J. Liu, C. Ko, R. Raghunathanan, J. Zhou, F. Oglertree, J. Li, J.C. Grossman, and J. Wu, *Sci. Rep.* 3, 2657 (2013).
- K. Matsuura, T. Ohashi, I. Muneta, S. Ishihara, N. Sawamoto, K. Kakushima, K. Tsutsui, A. Ogura, and H. Wakabayashi, *Semicond. Interface Spec. Conf. (SISC)* 3, 6 (2016).
- J. Tao, J. Chai, X. Lu, L.M. Wong, T.I. Wong, J. Pan, Q. Xiong, D. Chi, and S. Wang, *Nanoscale* 7, 2497 (2015).
- C.P. Lu, G. Li, J. Mao, L.-M. Wang, and E.Y. Andrei, *Nano Lett.* 14, 4628 (2014).
- W.A. West and A.W.C. Menzies, *J. Phys. Chem.* 33, 12 (1929).
- H. Li, Q. Zhang, C.C.R. Yap, B.K. Tay, T.H.T. Edwin, A. Olivier, and D. Baillargeat, *Adv. Funct. Mater.* 22, 1385 (2012).
- Z. Jin, S. Shin, D.H. Kwon, S.J. Han, and Y.S. Min, *Nanoscale* 6, 14453 (2014).
- X. Cui, G.H. Lee, Y.D. Kim, G. Arefe, P.Y. Huang, C.H. Lee, D.A. Chenet, X. Zhang, L. Wang, F. Ye, F. Pizzocchero, B.S. Jessen, K. Watanabe, T. Taniguchi, D.A. Muller, T. Low, P. Kim, and J. Hone, *Nat. Nanotechnol.* 10, 534 (2015).